BMC Medical Imaging

RESEARCH

Open Access

Preoperative MRI and CA19-9 for predicting occult lymph node metastasis in small pancreatic ductal adenocarcinoma (≤ 2 cm)

Qiying Tang[1†], Lei Li[2†], Zhiwei Pan[3†], Jianbo Li[3], Xiaolan Huang[1], Mengsu Zeng[3], Haitao Sun[3*] and Jianjun Zhou[1,3*]

Abstract

Aim Accurate prediction of occult lymph node metastasis (OLNM) in small pancreatic ductal adenocarcinoma (sPDAC) (≤ 2 cm) is crucial for curative management. This study aims to explore clinical and MRI features associated with OLNM in sPDAC and their pathological and prognostic implications.

Materials and methods This retrospective study included 135 patients with pathologically confirmed sPDAC who underwent surgery between September 2014 and September 2023. Preoperative multi-sequence MRI, clinical data, and pathological features were analyzed. Univariate and multivariate logistic regression models were used to identify risk predictors of OLNM in sPDAC. Receiver operating characteristic (ROC) analysis was performed to assess diagnostic performance and Kaplan-Meier survival analysis was used to evaluate prognostic outcomes.

Results OLNM was present in 43 (31.9%) sPDAC patients. Univariate and multivariate analysis identified elevated CA19-9 (> 100 U/mL) (OR = 2.404, $P = 0.040$) and low apparent diffusion coefficient (ADC) values (OR = 0.243, $P = 0.031$) as independent predictors of OLNM. The combined clinical-radiological model demonstrated an AUC of 0.740, significantly higher than CA19-9 (AUC = 0.653, $P = 0.021$) or ADC alone (AUC = 0.635, $P = 0.035$). sPDAC patients with OLNM exhibited higher rates of lymphovascular invasion (44.2%, $P = 0.013$) and pathological fat invasion (86.0%, $P = 0.030$). OLNM was associated with significantly worse OS and DFS ($P = 0.034$ and 0.043).

Conclusions OLNM is associated with adverse pathological features and poorer prognosis. The combination of preoperative MRI assessment of ADC and CA19-9 may aid in identifying sPDAC patients at high risk for OLNM.

Clinical trial number Not applicable.

Keywords Pancreatic ductal adenocarcinoma, Magnetic resonance imaging, Occult lymph node metastasis

†Qiying Tang, Lei Li and Zhiwei Pan contributed equally to this work. Haitao Sun and Jianjun Zhou are co-corresponding authors.

*Correspondence:
Haitao Sun
sht1720@163.com
Jianjun Zhou
zhoujianjunzs@126.com

[1]Department of Radiology, Zhongshan Hospital (Xiamen), Xiamen Municipal Clinical Research Center for Medical Imaging, Fudan University, No. 668 Jinhu Road, Huli District, Xiamen 361015, China
[2]Department of Radiology, Fengyang County People's Hospital, Chuzhou 233100, China
[3]Department of Radiology, Zhongshan Hospital, Shanghai Institute of Medical Imaging, Fudan University, No. 180 Fenglin Road, Xuhui District, Shanghai 200032, China

Introduction

Pancreatic ductal adenocarcinoma (PDAC) represents one of the most lethal solid tumors, with a 5-year survival rate below 10%, largely attributed to frequent late-stage diagnosis at initial presentations [1, 2]. Small PDAC (≤ 2 cm, sPDAC), often pertains to early-stage and potentially resectable, offers a curative window and exhibits markedly superior to advanced-stage disease [3, 4]. Nevertheless, up to 30% of these patients with small lesions still exhibit lymph node metastasis (LNM), resulting in substantially worsening postoperative overall survival (OS) and recurrence-free rates (RFS) [5]. This underscores the critical need for reliable preoperative LNM risk stratification in sPDAC [6, 7]. Importantly, accurate identification of LNM could directly impact clinical decision-making, particularly in selecting these early-stage patients for extended lymph node dissection or neoadjuvant chemotherapy to optimize outcomes [8].

Regrettably, more than 60% of pathologically confirmed metastatic lymph nodes measure less than 5 mm in size [9]. These small metastatic lymph nodes, defined as occult lymph node metastasis (OLNM), undetectable by standard preoperative imaging (rely on nodal size criteria), require postoperative histopathology for confirmation [10, 11]. Notably, in early-stage sPDAC, undetected OLNM leads to understaging, hindering treatment planning and prognosis [7]. Moreover, in sPDAC, the biological heterogeneity between primary tumor size and metastatic potential may result in disproportionate metastatic risk, implying that tumor size alone cannot reliably predict LNM in this population, aggravating the difficulty of preoperative evaluation [12]. Although the tumor marker carbohydrate antigen 19 – 9 (CA19-9) is known for its role in predicting tumor prognosis, its utility as an independent marker for LNM is hampered by limited sensitivity and specificity [13].

MRI has unique soft tissue resolution and multi-parameter imaging capabilities compared with CT, offering potential benefits in the assessment of biological behavior and prognosis of PDAC [14]. Furthermore, several functional MRI techniques, such as diffusion-weighted imaging (DWI) and dynamic contrast-enhanced (DCE) MRI, can reflect the heterogeneity of the tumor microenvironment through quantitative parameters, to some extent compensating for the limitations of traditional assessments that rely on lymph node and tumor size/morphology [15, 16]. Currently, most studies focus on analyzing the MRI characteristics of overall lymph node metastasis in pancreatic cancer patients [17, 18]. Research evaluating the risk of OLNM in sPDAC remains scarce. Critically, the combined predictive value of imaging features like ADC and clinical markers such as CA19-9 is poorly established, representing a key gap in preoperative risk stratification.

Preoperative OLNM risk assessment in sPDAC is crucial for staging, therapy, and prognosis. Thus, our study aimed to delineate the clinical and MRI features of sPDAC exhibiting OLNM, and their correlation with pathological characteristics and prognostic outcomes.

Materials and methods

This retrospective study was approved by the Institutional Review Committee of Zhongshan Hospital, Fudan university (No. B2024-250R) with a waiver of informed consent due to its retrospective nature. This study was performed in accordance with the Declaration of Helsinki and observed the Guidelines for Transparent Reporting of a Multivariable Prediction Model for Individual Prognosis or Diagnosis guidelines. Clinical trial number: not applicable.

A comprehensive review and selection process was conducted on patients diagnosed with pathologically verified PDAC spanning from September 2014 and September 2023. Subsequently, 135 eligible PDAC participants were included, meeting the predetermined enrollment standards: (a) pathologically and surgically confirmed sPDAC with a maximum diameter not exceeding 2 cm; (b) All enrolled patients had pathologically confirmed lymph node status, with no radiologically detected lymph node (short-axis diameter > 1 cm). (c) available preoperative multi-sequence MRI image encompassing pre-contrast T1-weighted image, three-phases contrast image, T2-weighted sequences, and diffusion-weighted imaging (DWI) and apparent diffusion coefficient (ADC) protocols; (d) accessible complete clinical-pathological data; (e) available follow-up information including OS and DFS. The criteria for inclusion and exclusion are outlined in Fig. 1.

MRI protocol

Given the prolonged timeline of the study, MRI scans were performed on different 1.5-T or 3.0-T MRI systems. Detailed information about the MRI protocols is provided in Table S1.

Clinical data analysis

The research evaluated an array of demographic and laboratory parameters, such as age, gender, body mass index (BMI), presence of diabetes, hypertension, serum concentrations of CA 19 – 9 and carcinoembryonic antigen (CEA), total bilirubin (TBil), and albumin levels.

Radiological features analysis

Two abdominal radiologists, with 10 and 23 years of experience in abdominal MRI respectively, performed a retrospective review of the imaging data without knowledge of additional clinical or pathological details. Each radiologist assessed the imaging characteristics of the

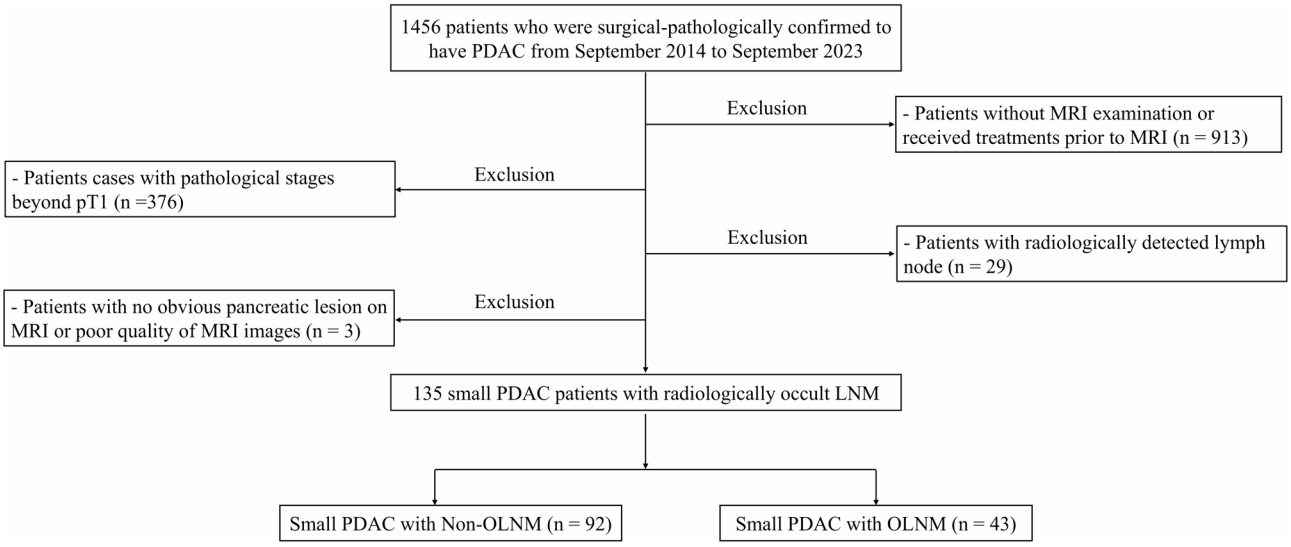

Fig. 1 The study selection flowchart illustrating patient inclusion and exclusion criteria

PDAC cases independently. Discrepancies in their evaluations were addressed by a third senior radiologist with 31 years of expertise in pancreatic MRI, who reviewed the images to achieve a final consensus.

As for qualitative MRI features, two independent reviewers independently and meticulously assessed the direct imaging features, including tumor site (head/uncinate or tail/body), margin (well-defined/ill-defined). Signal intensity on T2WI, diffusion-weighted (DWI), unenhanced T1WI, arterial (AP), portal venous (VP), and delayed phase (DP) sequences were categorized as hyp-, iso- or hyper-intense relative to the adjacent pancreatic parenchyma. Concomitant imaging findings, encompassing common bile duct dilatation, main pancreatic duct dilatation, and intrahepatic bile duct dilatation, superior mesenteric vein (SMV)/portal vein (PV) invasion, as well as pancreatic atrophy, peripancreatic fat invasion, cystic changes, necrosis, and rim enhancement, were recorded. The detailed image definition was described in Appendix S1.

For quantitative assessment, we measured the apparent diffusion coefficient (ADC) using DWI. To capture the most representative area of the tumor, we manually drew regions of interest (ROIs) on the images, focusing on the slice of where the tumor appeared largest. To minimize variability and increase confidence in our findings, three experienced radiologists independently measured the ADC, and we used the average of their measurements for our statistical analysis.

Pathological features analysis

Tumor staging, including pT and pN categories, was recorded based on the eighth edition of the American Joint Committee on Cancer (AJCC) staging system. Additionally, detailed pathological assessments, encompassing pathological grade, pathological fatty infiltration (PFI), lymphovascular invasion (LVI), peripheral nerve infiltration (PNI), and Ki-67 index, were also documented.

Prognosis data analysis

Prognostic data, including disease-free survival (DFS) and overall survival (OS), were recorded for evaluation. DFS refers to the time elapsed from the start of surgery to the detection of recurrence. Recurrence was classified into local relapses, new multicentric lesions, lymph node involvement, or distant metastatic spread. OS is characterized as the period from the date of surgery to either death from any cause or the most recent follow-up. The median OS and DFS follow-up period were 1.77 (interquartile range, 0.77–2.94) years and 1.01 (interquartile range, 0.51–2.20) years, respectively.

Statistical analysis

Continuous variables were presented as mean ± SD or median (IQR) based on normality determined by Shapiro-Wilk or Kolmogorov-Smirnov tests, with group comparisons performed using Student's t-test or Mann-Whitney U test, respectively. For the assessment of differences in clinical, pathological and radiological characteristics between two groups, t-test/Mann-Whitney U tests and chi-squared tests were applied. To explore the OLNM prediction potential of clinical and radiological features, both univariate and multivariate logistic regression models were constructed. Potential predictors were first screened using univariate analysis, and those with a P-value < 0.05 were included in a multivariate logistic regression model using a backward stepwise selection method to determine the final predictors, for which odds ratios (ORs) and 95% confidence intervals (CIs) were calculated. Receiver operating characteristic (ROC) analysis

was conducted to assess discriminative ability, with comparisons of the area under the curve (AUC) performed using DeLong's test. The impact of OLNM on small pancreatic cancer survival was evaluated using Kaplan-Meier survival analysis and log-rank tests for prognostic differences. The inter-rater reliability of MRI feature interpretations was quantified using Cohen's kappa (κ) or intraclass correlation coefficients (ICC), with agreement levels categorized as follows: 0.00–0.20, negligible; 0.21–0.40, slight; 0.41–0.60, intermediate; 0.61–0.80, substantial; and 0.81–1.00, almost perfect. A significant threshold of $P < 0.05$ was adopted for all statistical tests. All statistical analyses were executed using R (version 4.4.1).

Results

Patient characteristics

In this study, we performed a retrospective analysis of 1456 PDAC patients in our hospital between September 2014 and September 2023. Among them, 1321 were removed from the study population because they failed to meet the specified inclusion criteria (Fig. 1). Ultimately, 135 patients with sPDAC were included in this study. The median age of the cohort was 65.0 years (interquartile range [IQR], 59.0–69.0 years), with a female to male ratio of 59:76. Patients were subsequently categorized into non-OLNM ($n = 92$, 68.1%) and OLNM PDAC ($n = 43$, 31.9%) groups. Elevated CA19-9 (> 100 U/mL) was observed in 48.9% (66/135) of patients, with significantly higher proportions in OLNM of sPDAC patients (69.8%, 30/43) than non-OLNM of sPDAC patients (39.1%, 36/92; $P = 0.002$). Similarly, TBiL (> 22.2 μmol/L) occurred in 40.0% (54/135), again more frequently in OLNM (58.1%, 25/43) versus non-OLNM groups (31.5%, 29/92; $P = 0.006$). Analysis revealed that the OLNM groups did not differ significantly with respect to age, sex, BMI, diabetes, hypertension, albumin, CEA, and type of operation ($P = 0.197$–0.921; Table 1).

Radiological characteristics for predicting OLNM of sPDAC

Among the assessed imaging features, common bile duct dilatation and intrahepatic bile duct dilatation emerged as statistically significant predictors of OLNM in sPDAC. common bile duct dilatation was present in 45.9% patients (62/135), with a higher prevalence in the OLNM group (60.5%, 26/43) compared to the non-OLNM group (39.1%, 36/92) ($P = 0.033$). Similarly, intrahepatic bile duct dilatation was observed in 42.2% patients (57/135), with a markedly greater presence in the OLNM group (60.5%, 26/43) than in the non-OLNM group (33.7%, 31/92), demonstrating a stronger association ($P = 0.006$). Additionally, the apparent diffusion coefficient (ADC) showed a significant difference ($P = 0.012$), with a median value of 1.43 [IQR:1.24, 1.64] $\times 10^{-3}$ mm²/s across all patients, slightly higher in the non-OLNM group (1.49 [1.27, 1.79] $\times 10^{-3}$ mm²/s) compared to the OLNM group (1.4 [1.23, 1.55] $\times 10^{-3}$ mm²/s). In contrast, other radiological features did not exhibit statistically significant associations with OLNM (P values ranging from 0.220 to 0.885).

Interobserver agreement

The interobserver concordance for MRI features in sPDAC showed substantial agreement was observed for peripancreatic fat infiltration ($\kappa = 0.792$, 95% CI: 0.689–0.895), signal intensity in T1WI ($\kappa = 0.78$, 95% CI: 0.595–0.966), SMV/PV invasion ($\kappa = 0.731$, 95% CI: 0.564–0.897), and necrosis ($\kappa = 0.719$, 95% CI: 0.547–0.892), and almost perfect agreement across the remaining variables, with κ coefficients ranging from 0.822 to 0.941. For the ADC measurements, the ICC between the three radiologists ranged from 0.620 (95% confidence interval (CI): 0.505–0.714) to 0.783 (95% CI: 0.709–0.841), indicating substantial agreement (Table S2).

Univariate and multivariate analyses for risk clinical-radiological features between two groups

Univariate analysis revealed that high TBil (> 20.4 μmol/L), CA19-9 (> 100 U/mL), common bile duct dilatation, intrahepatic bile duct dilatation, and lower ADC values were significant predictors of OLNM in sPDAC, with ORs ranging from 0.204 to 3.59 ($P = 0.001$–0.022). In multivariate analysis, High CA19-9 level (> 100 U/mL) (OR = 2.404, 95% CI: 1.051–5.666, $P = 0.040$) and low ADC values (OR = 0.243, 95% CI: 0.061–0.814, $P = 0.031$) remained significant, suggesting their independent predictive value (Table 2). Other clinical factors, including age, BMI, sex, diabetes, hypertension, and various imaging features (e.g., tumor location, margin) were non-significant ($P = 0.096$–0.921) (Figs. 2 and 3).

Building on these findings, a combined clinical-radiological predictor was developed, showing the significantly elevated AUC of 0.740, outperforming CA19-9 alone (AUC = 0.653, $P = 0.021$) and ADC alone (AUC = 0.635, threshold value = 1.597×10^3 mm²/s, $P = 0.035$) in predicting OLNM of sPDAC (Table 3; Fig. 4).

Pathological features and prognostic outcomes in sPDAC with occult lymph node metastasis

As for pathological features analysis, several significant pathological differences were observed between groups (Table 4). Among patients with sPDAC undergoing OLNM, pN1 metastasis was predominant (86.0%, 37/43), followed by pN2 (14.0%, 6/43); all non-OLNM cases were classified as pN0. Similarly, most of these patients were classified as AJCC stage II (86.0%, 37/43), with the remaining 14.0% (6/43) categorized as stage III. Moreover, patients in OLNM group showed higher LVI (44.2% vs. 21.7%, $P = 0.013$) and PFI (86.0% vs. 68.5%, $P = 0.030$),

Table 1 The baseline clinical-radiological features in sPDAC

Characteristic	All (*N* = 135)	Non-OLNM (*N* = 92)	OLNM (*N* = 43)	*P*-value
Clinical features				
Age (years)	65.0 [59.0, 69.0]	66.0 [59.0, 69.5]	65.0 [59.0, 68.0]	0.489
BMI (kg/m^2)	22.6 [20.5, 24.2]	22.7 [20.7, 24.3]	22.5 [20.3, 23.8]	0.187
Sex				0.393
Female	59 (43.7%)	43 (46.7%)	16 (37.2%)	
Male	76 (56.3%)	49 (53.3%)	27 (62.8%)	
Diabetes				0.906
Absence	98 (72.6%)	66 (71.7%)	32 (74.4%)	
Presence	37 (27.4%)	26 (28.3%)	11 (25.6%)	
Hypertension				0.536
Absence	78 (57.8%)	51 (55.4%)	27 (62.8%)	
Presence	57 (42.2%)	41 (44.6%)	16 (37.2%)	
TBil (μmol/L)				0.006
≤ 20.4	81 (60.0%)	63 (68.5%)	18 (41.9%)	
> 20.4	54 (40.0%)	29 (31.5%)	25 (58.1%)	
Albumin (g/L)				0.921
≤ 37	126 (93.3%)	86 (93.5%)	40 (93.0%)	
> 37	9 (6.7%)	6 (6.5%)	3 (7.0%)	
CA19-9 (U/mL)				0.002
≤ 100	69 (51.1%)	56 (60.9%)	13 (30.2%)	
> 100	66 (48.9%)	36 (39.1%)	30 (69.8%)	
CEA (ng/mL)				0.678
≤ 5	108 (80.0%)	75 (81.5%)	33 (76.7%)	
> 5	27 (20.0%)	17 (18.5%)	10 (23.3%)	
Type of Operation				0.219
Pancreatoduodenectomy	89 (65.9%)	57 (62.0%)	32 (74.4%)	
Distal pancreatectomy	46 (34.1%)	35 (38.0%)	11 (25.6%)	
Radiological features				
Tumor Location				0.707
head/uncinate	96 (71.1%)	64 (69.6%)	32 (74.4%)	
tail/body	39 (28.9%)	28 (30.4%)	11 (25.6%)	
Margin				0.630
Well-defined	76 (56.3%)	50 (54.3%)	26 (60.5%)	
Ill-defined	59 (43.7%)	42 (45.7%)	17 (39.5%)	
Rim Enhancement				0.553
Absence	88 (65.2%)	62 (67.4%)	26 (60.5%)	
Presence	47 (34.8%)	30 (32.6%)	17 (39.5%)	
Signal in T2WI				0.525
Iso-/hypointense	59 (43.7%)	38 (41.3%)	21 (48.8%)	
Hyperintense	76 (56.3%)	54 (58.7%)	22 (51.2%)	
Signal in DWI				0.553
Iso-/hypointense	47 (34.8%)	30 (32.6%)	17 (39.5%)	
Hyperintense	88 (65.2%)	62 (67.4%)	26 (60.5%)	
Signal in T1WI				0.395
Iso-/hyper-intense	13 (9.6%)	7 (7.6%)	6 (14.0%)	
Hypointense	122 (90.4%)	85 (92.4%)	37 (86.0%)	
Signal in AP				0.487
Iso-/hyper-intense	35 (25.9%)	26 (28.3%)	9 (20.9%)	
Hypointense	100 (74.1%)	66 (71.7%)	34 (79.1%)	
Signal in VP				0.606
Iso-/hyper-intense	75 (55.6%)	53 (57.6%)	22 (51.2%)	
Hypointense	60 (44.4%)	39 (42.4%)	21 (48.8%)	

Table 1 (continued)

Characteristic	All (*N* = 135)	Non-OLNM (*N* = 92)	OLNM (*N* = 43)	*P*-value
Signal in DP				0.325
Iso-/hyper-intense	97 (71.9%)	69 (75.0%)	28 (65.1%)	
Hypointense	38 (28.1%)	23 (25.0%)	15 (34.9%)	
Common Bile Duct Dilatation				0.033
Absence	73 (54.1%)	56 (60.9%)	17 (39.5%)	
Presence	62 (45.9%)	36 (39.1%)	26 (60.5%)	
Intrahepatic Bile Duct Dilatation				0.006
Absence	78 (57.8%)	61 (66.3%)	17 (39.5%)	
Presence	57 (42.2%)	31 (33.7%)	26 (60.5%)	
Main Pancreatic Duct Dilatation				0.472
Absence	45 (33.3%)	33 (35.9%)	12 (27.9%)	
Presence	90 (66.7%)	59 (64.1%)	31 (72.1%)	
SMV/PV Invasion				0.885
Absence	117 (86.7%)	80 (87.0%)	37 (86.0%)	
Presence	18 (13.3%)	12 (13.0%)	6 (14.0%)	
Pancreatic Tail Atrophy				0.245
Absence	83 (61.5%)	53 (57.6%)	30 (69.8%)	
Presence	52 (38.5%)	39 (42.4%)	13 (30.2%)	
Peripancreatic Fat Infiltration				0.220
Absence	59 (43.7%)	44 (47.8%)	15 (34.9%)	
Presence	76 (56.3%)	48 (52.2%)	28 (65.1%)	
Necrosis				0.818
Absence	119 (88.1%)	82 (89.1%)	37 (86.0%)	
Presence	16 (11.9%)	10 (10.9%)	6 (14.0%)	
Cystic Degeneration				0.225
Absence	117 (86.7%)	77 (83.7%)	40 (93.0%)	
Presence	18 (13.3%)	15 (16.3%)	3 (7.0%)	
ADC ($\times 10^{-3}$ mm^2/s)	1.43 [1.24, 1.64]	1.49 [1.27, 1.79]	1.4 [1.23, 1.55]	0.012

sPDAC = small pancreatic ductal adenocarcinoma, OLNM = occult lymph node metastasis, BMI = body mass index; TBil = total bilirubin, CA 19 – 9 = cancer antigen 19 – 9, CEA = carcinoembryonic antigen, DWI = diffusion weight imaging, AP = arterial phase, VP = venous phase, DP = delayed phase, SMV = superior mesenteric vein, PV = portal vein, ADC = apparent diffusion coefficient

while PNI was similar ($P = 0.270$). Other pathological factors, including SMAD4 mutation, pathological grade, and Ki-67 index, showed no significant differences ($P = 0.160$–0.904, respectively).

For prognostic analysis, in our study, sPDAC with OLNM demonstrated significantly worse OS and DFS rates compared to those with non-OLNM ($P = 0.034$ and 0.043, respectively). Detailed analysis revealed that 1-, 3-, and 5-year OS rates for sPDAC patients with OLNM were 77.7%, 55.8%, and 25.8%, compared to 86.7%, 55.8%, and 47.4% for patients with non-OLNM (Fig. 5a). Consistent with these findings, the 1-, 3-, and 5-year DFS rates were also lower in the OLNM group (47.7%, 33.7%, and 14.5%) than in the non-OLNM group (70.2%, 43.8%, and 39.9%) (Fig. 5b).

Discussion

In this study, we investigated the clinical and MRI predictive features associated with OLNM in sPDAC (≤ 2 cm) and determined their implications for pathology and prognosis. The findings revealed that sPDAC with OLNM displayed a more aggressive biological phenotype, characterized by significantly higher rates of LVI (44.2%) and PFI (86.0%), as well as poor OS and DFS, compared to those with non-OLNM. Additionally, elevated CA19-9 levels (OR = 2.404,) and low ADC values (OR = 0.243) emerged as independently significant predictors of OLNM in sPDAC patients. Notably, the combination of CA19-9 and ADC values demonstrates the best discriminatory power (AUC = 0.740) compared to individual markers.

Although LNM in PDAC has been widely studied, OLNM in sPDAC (≤ 2 cm) remains underexplored. In PDAC broadly, radiologically detected lymph node and tumor size are key preoperative LNM risk indicators [19, 20]. However, in this early stage sPDAC cohort, evaluating preoperatively radiologically occult lymph node metastasis presents distinct clinical challenges [21, 22]. In our cohort, sPDAC with OLNM exhibited more aggressive pathological features, including higher rates of LVI

Table 2 Univariate and multivariate analyses for clinical-radiological predictors for OLNM of sPDAC

Characteristics	Univariate analysis				Multivariate analysis			
	OR	CI_lower	CI_upper	P	OR	CI_lower	CI_upper	P
Age	0.984	0.948	1.021	0.392				
BMI (kg/m^2)	0.887	0.766	1.017	0.096				
Sex [Male]	1.481	0.711	3.154	0.300				
Diabetes [presence]	0.873	0.373	1.952	0.745				
Hypertension [presence]	0.737	0.346	1.538	0.421				
TBil [> 20.4 μmol/L]	3.017	1.438	6.466	0.004	1.878	0.602	5.916	0.274
Albumin [> 37 g/L]	1.075	0.218	4.295	0.921				
CA19-9 [> 100 U/mL]	3.59	1.685	7.988	0.001	2.404	1.051	5.666	0.040
CEA	1.337	0.539	3.194	0.519				
Type of Operation [Pancreatoduodenectomy]	0.56	0.243	1.225	0.157				
Tumor Location [head/uncinate]	0.786	0.337	1.746	0.563				
Margin [Ill-defined]	0.778	0.368	1.617	0.505				
Rim enhancement [presence]	1.351	0.632	2.858	0.432				
Signal in T2WI [hyperintense]	0.737	0.355	1.53	0.412				
Signal in DWI [hyperintense]	0.74	0.35	1.581	0.432				
Signal in T1WI [hypointense]	0.508	0.158	1.675	0.251				
Signal in AP [hypointense]	1.488	0.644	3.684	0.367				
Signal in VP [hypointense]	1.297	0.626	2.692	0.483				
Signal in DP [hypointense]	1.607	0.726	3.516	0.236				
Common Bile Duct Dilatation [presence]	2.379	1.143	5.062	0.022	0.322	0.014	2.769	0.365
Intrahepatic Bile Duct Dilatation [presence]	3.009	1.436	6.46	0.004	5.252	0.59	118.794	0.183
Main Pancreatic Duct Dilatation [presence]	1.445	0.666	3.272	0.362				
SMV/PV Invasion [presence]	1.081	0.353	3.015	0.885				
Pancreatic Tail Atrophy [presence]	0.589	0.266	1.255	0.178				
Peripancreatic Fat Infiltration [presence]	1.711	0.818	3.681	0.160				
Necrosis [presence]	1.33	0.425	3.859	0.606				
Cystic Degeneration [presence]	0.385	0.086	1.252	0.149				
ADC ($\times 10^{-3}$ mm^2/s)	0.204	0.06	0.593	0.006	0.243	0.061	0.814	0.031

sPDAC = small pancreatic ductal adenocarcinoma, OLNM = occult lymph node metastasis, BMI = body mass index; TBil = total bilirubin, CA 19 − 9 = cancer antigen 19 − 9, CEA = carcinoembryonic antigen, DWI = diffusion weight imaging, AP = arterial phase, VP = venous phase, DP = delayed phase, SMV = superior mesenteric vein, PV = portal vein, ADC = apparent diffusion coefficient

and PFI, reflecting greater invasiveness. Additionally, the OLNM group demonstrated a 1.85-fold increased risk of 5-year mortality and a 2.78-fold worse DFS compared to the non-OLNM group. Insufficient recognition of OLNM can lead to understaging, suboptimal treatment, and adverse prognostic outcomes, underscoring its clinical significance [23]. These findings strengthen lymph node involvement, even when occult at early stage, is a key determinant of recurrence and mortality in PDAC, reinforcing the need for early identification to guide therapeutic strategies, such as extended lymphadenectomy or neoadjuvant therapy, which have shown promise in improving outcomes in node-positive PDAC [24].

Even when undetectable via standard size-threshold imaging protocols, MRI with its superior multisequence and functional imaging capabilities offers distinct advantages over CT in characterizing PDAC behavior [25]. DWI facilitates the observation of water molecule diffusion at a microscopic level, offering valuable information about tumor vitality and microstructural characteristics [26]. In the context of hepato-biliary-pancreatic malignancies, reduced ADC values have been linked to increased tumor grade, poor cellular differentiation, and unfavorable prognosis, serving as a broad indicator of tumor aggressiveness [27, 28]. Ju Hee Lee et al. have demonstrated that the ADC values of metastatic lymph nodes in pancreaticobiliary cancers are significantly lower than those of non-metastatic lymph nodes [20]. While direct ADC measurement is not feasible in patients with OLNM, these results highlight the potential of ADC as a diagnostic tool for assessing the risk of LNM. Another prior research demonstrated that diffusion kurtosis imaging (DKI)-derived mean diffusivity (MD) was significantly reduced in PDAC accompanied by small LNM, suggesting microstructural changes correlated with metastatic progression [29]. Our study confirms that the DWI-derived ADC value is an independent predictor of OLNM in sPDAC, likely by reflecting the tumor's

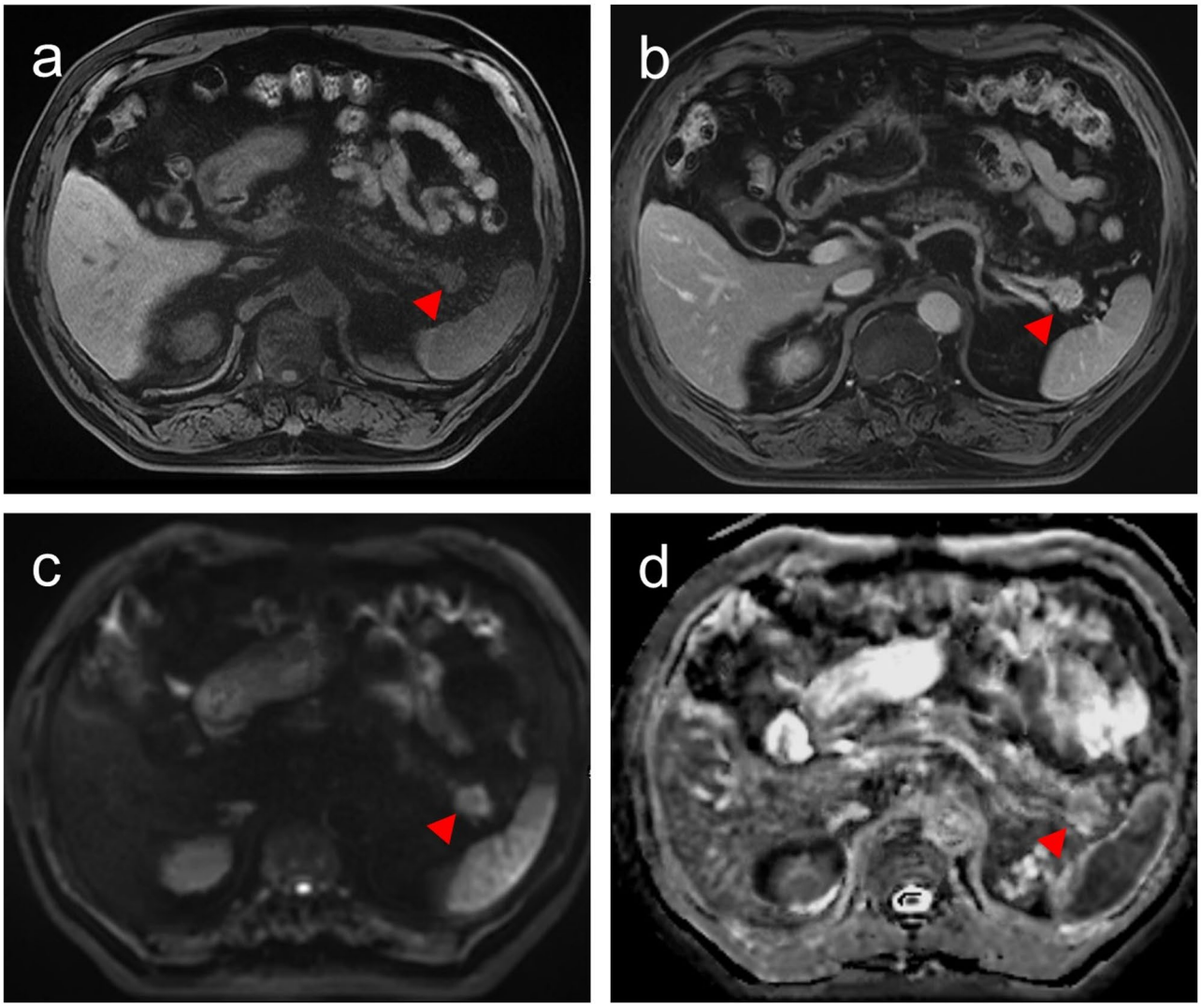

Fig. 2 A patient with a 1.3-cm pancreatic ductal adenocarcinoma, baseline CA19-9: 14.7 U/mL, stage pT1N0M0. (**a**) Pre-contrast T1WI image shows a hypointense mass (red triangle). (**b**) The T1WI in delayed phase exhibits relative hyperintense. (**c**) Diffusion-weighted image (b = 500 s/mm^2) shows a hyperintense mass (red triangle). (**d**) The apparent diffusion coefficient (ADC) map exhibits relative hypointensity (mean ADC = 1.726×10^3 mm^2/s; red triangle)

underlying aggressive biological behavior and playing a significant role in its preoperative evaluation. Moreover, further research integrating advanced functional MRI parameters such as IVIM and DKI holds promise for providing even more nuanced insights into the microstructural changes associated with OLNM.

In addition to functional MRI parameters, conventional qualitative features including common bile duct and intrahepatic bile duct dilatation are more frequent in sPDAC with OLNM, potentially reflecting a more invasive growth pattern. While these qualitative features were significant in univariate analysis, their predictive value diminished in the multivariate model, suggesting that qualitative features may have limited ability to capture underlying tumor biology in patients with early-stage small lesions. Besides, while other MRI features such as T2 signal intensity, rim enhancement, etc., were also evaluated, ADC proved to be the most robust independent risk factor.

CA19-9 level, a clinically validated marker for aggressive PDAC, is strongly associated with tumor staging, disease progression and the likelihood of metastasis [30]. Multiple studies have demonstrated that elevated preoperative CA19-9 levels are associated with an increased likelihood of lymph node metastasis in resectable pancreatic adenocarcinoma [31, 32]. Jianchen Ge and colleagues identified CA19-9 as an independent predictor of occult metastasis in pancreatic cancer [33]. Another meta-analysis revealed that preoperative mean CA19-9 levels were significantly elevated in patients with metastatic pancreatic cancer compared to those without metastasis; however, a consensus on the optimal cutoff

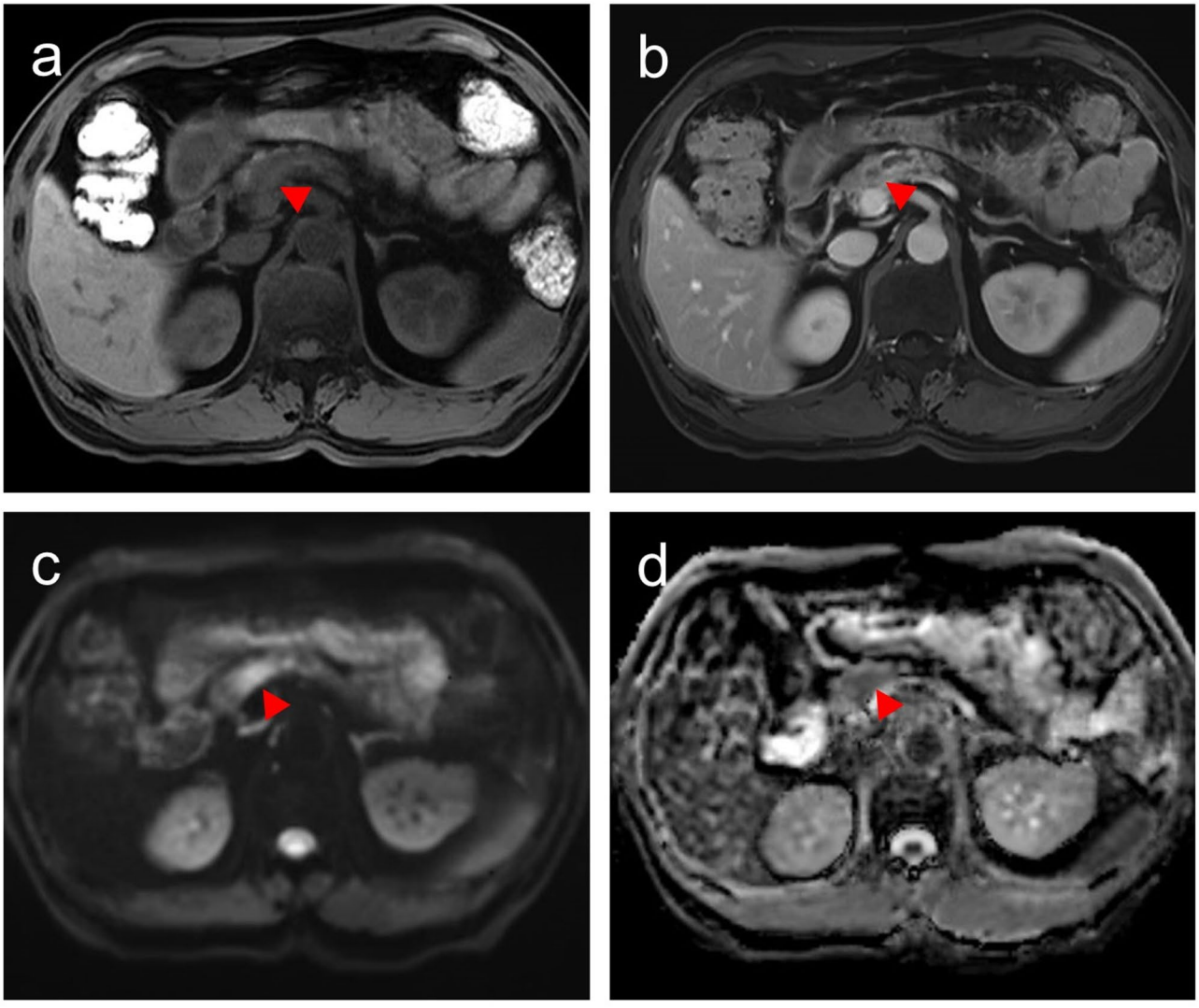

Fig. 3 A patient with a 1.5-cm pancreatic ductal adenocarcinoma, baseline CA19-9 111.6 U/mL, stage pT1N1M0. (**a**) Pre-contrast T1WI shows a hypointense mass (red triangle). (**b**) The T1WI in delayed phase exhibits relative hypointense. (**c**) Diffusion-weighted image (b = 500 s/mm^2) shows a hyperintense mass (red triangle). (**d**) The apparent diffusion coefficient (ADC) map exhibits relative hypointensity (mean ADC = 1.248 × 10^3 mm^2/s; red triangle)

Table 3 Predictive performance of the risk clinical-radiological features for OLNM in sPDAC

Parameters	AUC	*P* value	Threshold	Sensitivity	Specificity	PPV	NPV
Combined	0.740	NA	NA	0.837	0.565	0.474	0.881
CA19-9	0.653	0.021	NA	0.698	0.609	0.455	0.812
ADC	0.635	0.035	1.597(×10^3 mm^2/s)	0.907	0.391	0.411	0.900

sPDAC = small pancreatic ductal adenocarcinoma, OLNM = occult lymph node metastasis, AUC = area under the curve; PPV = Positive Predictive Value NPV = Negative Predictive Value; ADC = apparent diffusion coefficient; NA = not applicable

threshold remains elusive. In line with these findings, our results affirm that an elevated CA19-9 level is a powerful independent clinical predictor for OLNM in sPDAC. More importantly, the further combination of CA19-9 and ADC outperformed individual predictors, suggesting a synergistic role for these markers in OLNM risk assessment in sPDAC. Elevated CA19-9 likely indicates systemic tumor burden and metastatic potential, while ADC offers localized insights into the tumor microenvironment. This integrated clinical-radiological model addresses the key limitation of size-based imaging by combining functional MRI parameters with serological biomarkers, which enables more accurate evaluation of tumor biology, reducing understaging rates and optimizing patient selection for intensive therapies.

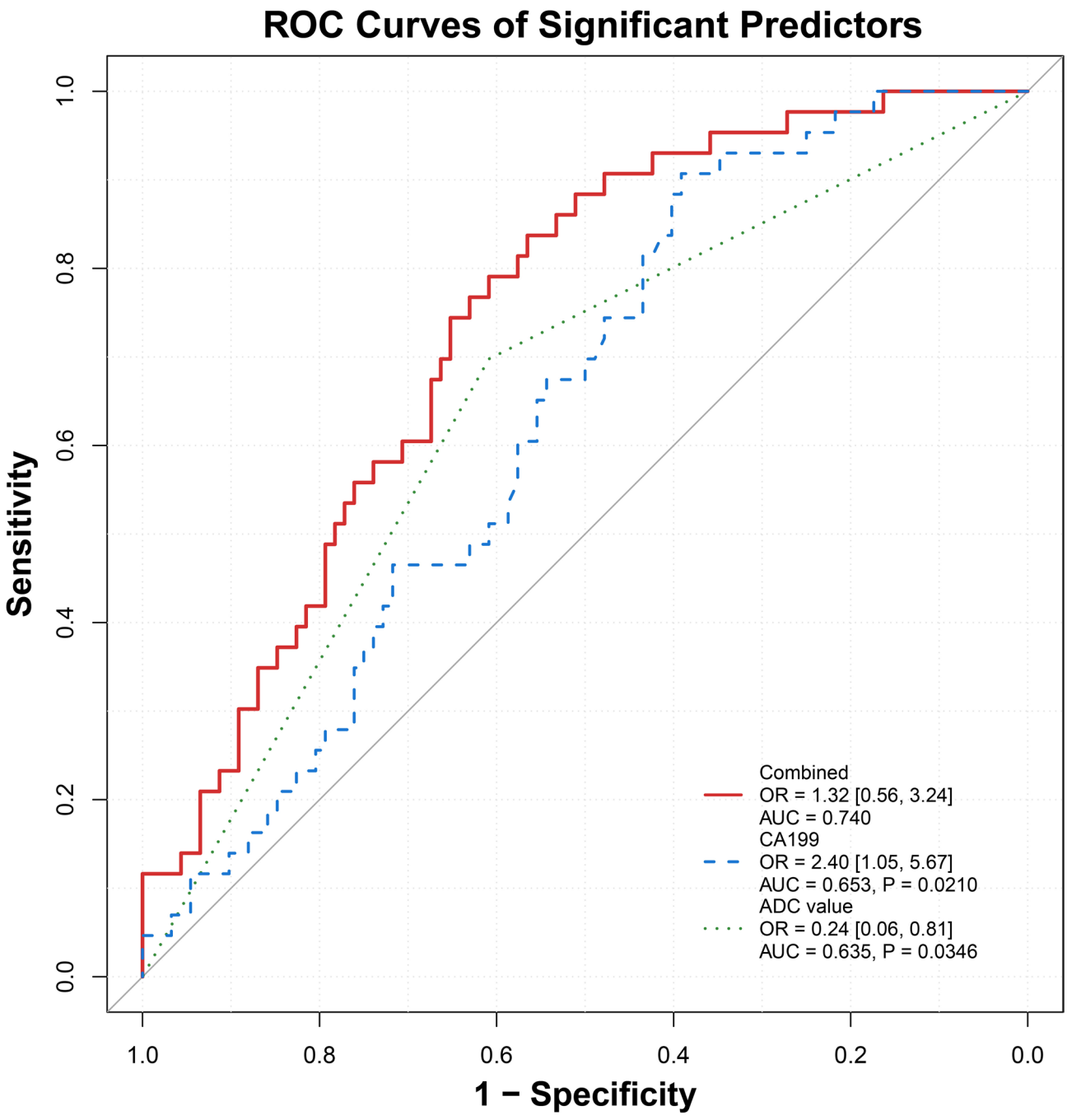

Fig. 4 ROC curves for predicting occult lymph node metastasis (OLNM) in small PDAC patients for single and combined clinical-radiological parameters

There are several limitations in this study. First, due to the limited number of participants from single-center and the potential for selection bias inherent in its retrospective nature, the findings necessitate validation through a more extensive investigation. Second, our study only employed standard DWI and ADC, excluding advanced functional imaging techniques. However, the use of standard quantitative functional MRI parameters eliminated the need for specialized hardware or proprietary software, potentially enhancing its clinical accessibility and routine application. Next, the use of data acquired over a long period from various MRI scanners (both 1.5T and 3.0T), which introduces potential variability in ADC measurements. Consequently, our findings require robust validation in multi-center, multi-protocol settings to ensure their broader applicability and reproducibility. Lastly, the participants from only single center were analyzed in this study. Subsequent multi-institutional investigations incorporating external validation cohorts are essential.

Table 4 Analysis of pathologic features associated with OLNM in sPDAC

Characteristic	All (*N* = 135)	Non-OLNM (*N* = 92)	OLNM (*N* = 43)	*P*-value
SMAD4 Mutation				0.777
Negative	51 (37.8%)	36 (39.1%)	15 (34.9%)	
Positive	84 (62.2%)	56 (60.9%)	28 (65.1%)	
Pathological Grade				0.160
Well/moderate-differentiated	70 (51.9%)	52 (56.5%)	18 (41.9%)	
Ill-differentiated	65 (48.1%)	40 (43.5%)	25 (58.1%)	
Ki-67 index				0.904
Low	92 (68.1%)	63 (68.5%)	29 (67.4%)	
High	43 (31.9%)	29 (31.5%)	14 (32.6%)	
LVI				0.013
Absence	96 (71.1%)	72 (78.3%)	24 (55.8%)	
Presence	39 (28.9%)	20 (21.7%)	19 (44.2%)	
PNI				0.270
Absence	28 (20.7%)	22 (23.9%)	6 (14.0%)	
Presence	107 (79.3%)	70 (76.1%)	37 (86.0%)	
PFI				0.030
Absence	35 (25.9%)	29 (31.5%)	6 (14.0%)	
Presence	100 (74.1%)	63 (68.5%)	37 (86.0%)	

sPDAC = small pancreatic ductal adenocarcinoma, OLNM = occult lymph node metastasis, LVI = lymphovascular invasion, PNI = peripheral nerve infiltration, PFI = pathological fatty infiltration

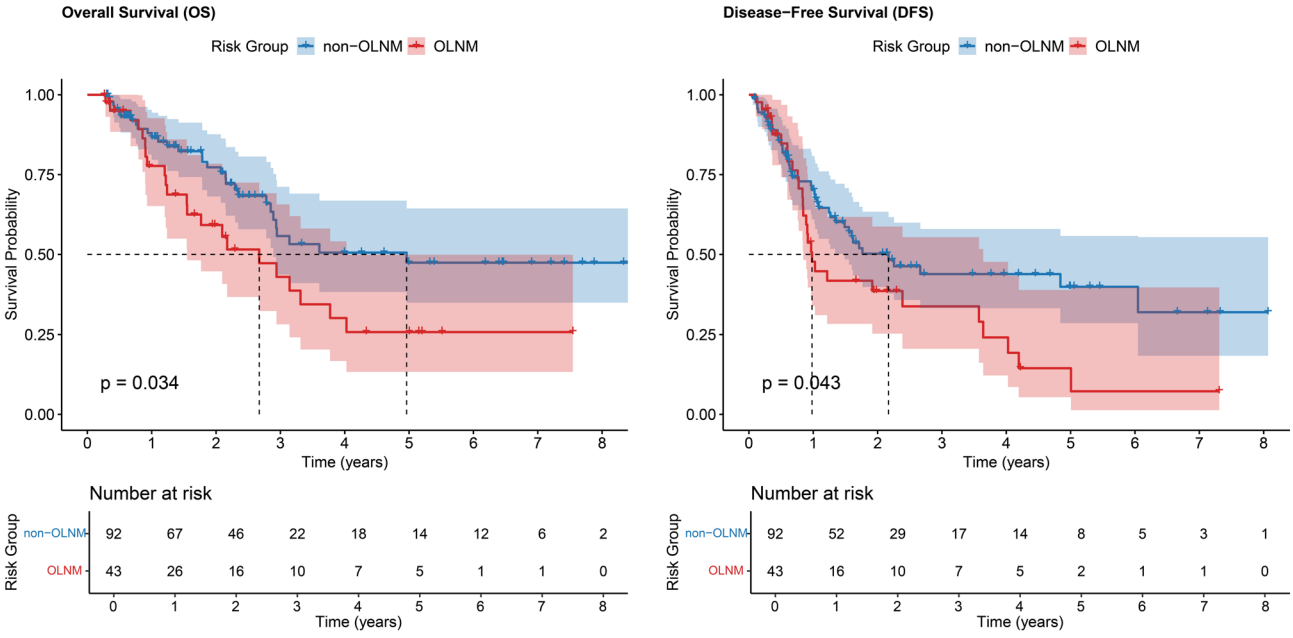

Fig. 5 Kaplan-Meier survival analysis comparing overall survival (OS) and disease-free survival (DFS) between small PDAC patients with occult lymph node metastasis (OLNM) and non-OLNM patients. Small PDAC patients with OLNM demonstrated significantly worse OS (**a**) and DFS (**b**) compared to non-OLNM patients (*P* = 0.034 and 0.043, respectively)

In summary, our study demonstrates that sPDACs with OLNM display aggressive tumor biology, characterized by adverse pathological features (including PFI and LVI) and significantly worse OS and DFS rates. Elevated CA19-9 levels and reduced ADC values correlated with OLNM in sPDAC, and their combination demonstrated optimal predictive performance. Therefore, integrated clinical and MRI features may refine OLNM identification in early-stage sPDAC, critically informing aggressive treatment strategies, such as extended lymphadenectomy, or neoadjuvant chemotherapy for improved oncological outcomes.

Abbreviations

sPDAC	Small Pancreatic Ductal Adenocarcinoma
OLNM	Occult Lymph Node Metastasis
ADC	Apparent Diffusion Coefficient
OS	Overall Survival
RFS	Recurrence-Free Rates
DFS	Disease-Free Survival
CA19-9	carbohydrate antigen 19 – 9
DWI	Diffusion-Weighted Imaging
AP	Arterial Phase
VP	Venous Phase
DP	Delayed Phase
SMV	Superior Mesenteric Vein
PV	Portal Vein
ROC	Receiver Operating Characteristic
AUC	Area Under the Curve
OR	Odds Ratio
CIs	confidence intervals
BMI	Body Mass Index
CEA	Carcinoembryonic Antigen
TBil	Total Bilirubin
ROI	Region of Interest
AJCC	American Joint Committee on Cancer
PFI	Pathological Fatty Infiltration
LVI	Lymphovascular Invasion
PNI	Peripheral Nerve Infiltration
ICC	Intraclass Correlation Coefficient
IQR	Interquartile Range
PPV	Positive Predictive Value
NPV	Negative Predictive Value
DKI	Diffusion Kurtosis Imaging
MD	Mean Diffusivity
CI	Confidence Interval

Supplementary Information

The online version contains supplementary material available at https://doi.org/10.1186/s12880-025-01854-3.

Supplementary Material 1

Acknowledgements
Not applicable.

Author contributions
All authors contributed to the study conception and design. Qiying Tang, Lei Li, and Zhiwei Pan wrote the main manuscript text and Qiying Tang, Lei Li, Zhiwei Pan, and Haitao Sun prepared figures. Material preparation, data collection and analysis were performed by Qiying Tang, Lei Li, Zhiwei Pan, Jianbo Li, Xiaolan Huang, Mengsu Zeng, and Haitao Sun. Jianjun Zhou and Haitao Sun supervised the study and is the guarantor. All authors reviewed the manuscript.

Funding
This work was funded by the Shanghai Municipal Health Commission Health Industry Clinical Research Special Program (Youth Project) (20244Y0003) and the Health and Technology Project of Fujian Province (2022QNB020).

Data availability
The datasets used and/or analyzed during the present study are available from the corresponding author on reasonable request.

Declarations

Ethics approval and consent to participate
This retrospective study was approved by the ethics committee of Zhongshan Hospital, Fudan university (B2024-250R), which waived the requirement for written informed consent owing to the use of deidentified retrospective data. This study was performed in accordance with the Declaration of Helsinki.

Consent for publication
Not applicable.

Competing interests
The authors declare no competing interests.

Received: 13 April 2025 / Accepted: 29 July 2025
Published online: 06 August 2025

References

1. Conroy T, Pfeiffer P, Vilgrain V, Lamarca A, Seufferlein T, O'Reilly EM, Hackert T, Golan T, Prager G, Haustermans K, et al. Pancreatic cancer: ESMO clinical practice guideline for diagnosis, treatment and follow-up. Ann Oncol. 2023;34(11):987–1002.
2. Iacobuzio-Donahue CA. The war on pancreatic cancer: progress and promise. Nat Rev Gastro Hepat. 2023;20(2):75–6.
3. Fyfe I. AI predicts pancreatic cancer risk. Nat Rev Gastro Hepat. 2023;20(7):413.
4. Yurgelun MB. Building on more than 20 years of progress in pancreatic cancer surveillance for High-Risk individuals. J Clin Oncol. 2022;40(28):3230–4.
5. Stoffel EM, Brand RE, Goggins M. Pancreatic Cancer: Changing Epidemiology and New Approaches to Risk Assessment, Early Detection, and Prevention. *Gastroenterology* 2023, 164(5):752–765.
6. Katz MH, Hwang R, Fleming JB, Evans DB. Tumor-node-metastasis staging of pancreatic adenocarcinoma. Ca-cancer J Clin. 2008;58(2):111–25.
7. Fink DM, Steele MM, Hollingsworth MA. The lymphatic system and pancreatic cancer. Cancer Lett. 2016;381(1):217–36.
8. Nishiwada S, Sho M, Banwait JK, Yamamura K, Akahori T, Nakamura K, Baba H, Goel A. A MicroRNA signature identifies pancreatic ductal adenocarcinoma patients at risk for lymph node metastases. Gastroenterology. 2020;159(2):562–74.
9. Prenzel KL, Hölscher AH, Vallböhmer D, Drebber U, Gutschow CA, Mönig SP, Stippel DL. Lymph node size and metastatic infiltration in adenocarcinoma of the pancreatic head. Ejso-eur J Surg Onc. 2010;36(10):993–6.
10. Wang Z, Wu Y, Wang L, Gong L, Han C, Liang N, Li S. Predicting occult lymph node metastasis by nomogram in patients with lung adenocarcinoma =2 cm</at. Future Oncol. 2021;17(16):2005–13.
11. Ma D, Zhang Y, Shao X, Wu C, Wu J. PET/CT for predicting occult lymph node metastasis in gastric cancer. Curr Oncol. 2022;29(9):6523–39.
12. Shin J, Shin S, Lee JH, Song KB, Hwang DW, Kim HJ, Byun JH, Cho H, Kim SC, Hong S. Lymph node size and its association with nodal metastasis in ductal adenocarcinoma of the pancreas. J Pathol Transl Med. 2020;54(5):387–95.
13. Raza SS, Khan H, Hajibandeh S, Hajibandeh S, Bartlett D, Chatzizacharias N, Roberts K, Marudanayagam R, Sutcliffe RP. Can preoperative carbohydrate antigen 19– 9 predict metastatic pancreatic cancer? Results of a systematic review and meta-analysis. HPB. 2024;26(5):630–8.
14. Lee S, Kim SH, Park HK, Jang KT, Hwang JA, Kim S. Pancreatic Ductal Adenocarcinoma: Rim Enhancement at MR Imaging Predicts Prognosis after Curative Resection. *Radiology* 2018, 288(2):456–466.
15. Shin N, Kang TW, Min JH, Hwang JA, Kim YK, Kim Y, Han IW, Kim K. Utility of Diffusion-Weighted MRI for detection of locally recurrent pancreatic cancer after surgical resection. Am J Roentgenol. 2022;219(5):762–73.
16. Ottens T, Barbieri S, Orton MR, Klaassen R, van Laarhoven HWM, Crezee H, Nederveen AJ, Zhen X, Gurney-Champion OJ. Deep learning DCE-MRI parameter estimation: application in pancreatic cancer. Med Image Anal. 2022;80:102512.
17. Shi L, Wang L, Wu C, Wei Y, Zhang Y, Chen J. Preoperative prediction of lymph node metastasis of pancreatic ductal adenocarcinoma based on a radiomics nomogram of Dual-Parametric MRI imaging. Front Oncol. 2022;12:927077.
18. Zeng P, Qu C, Liu J, Cui J, Liu X, Xiu D, Yuan H. Comparison of MRI and CT-based radiomics for preoperative prediction of lymph node metastasis in pancreatic ductal adenocarcinoma. Acta Radiol. 2023;64(7):2221–8.
19. Guo X, Song X, Long X, Liu Y, Xie Y, Xie C, Ji B. New nomogram for predicting lymph node positivity in pancreatic head cancer. Front Oncol 2023, 13:1053375
20. Lee JH, Han S, Hong EK, Cho HJ, Joo J, Park EY, Woo SM, Kim TH, Lee WJ, Park S. Predicting lymph node metastasis in pancreatobiliary cancer with magnetic resonance imaging: A prospective analysis. Eur J Radiol. 2019;116:1–7.
21. Li D, Hu B, Zhou Y, Wan T, Si X. Impact of tumor size on survival of patients with resected pancreatic ductal adenocarcinoma: a systematic review and meta-analysis. BMC Cancer 2018, 18(1).

22. Yee EJ, Torphy RJ, Thielen ON, Easwaran L, Franklin O, Sugawara T, Bartsch C, Garduno N, McCarter MM, Ahrendt SA, et al. Radiologic occult metastases in pancreatic cancer: analysis of risk factors and survival outcomes in the age of contemporary neoadjuvant Multi-agent chemotherapy. Ann Surg Oncol. 2024;31(9):6127–37.
23. Reiser Erkan C, Gaa J, Kleeff J. T1 pancreatic cancer with lymph node metastasis and perineural invasion of the Celiac trunk. Clin Gastroenterol H. 2008;6(11):e41–2.
24. Kang MJ, Jang JY, Kim SW. Surgical resection of pancreatic head cancer: what is the optimal extent of surgery? Cancer Lett. 2016;382(2):259–65.
25. De Robertis R, Beleu A, Cardobi N, Frigerio I, Ortolani S, Gobbo S, Maris B, Melisi D, Montemezzi S, D'Onofrio M. Correlation of MR features and histogram-derived parameters with aggressiveness and outcomes after resection in pancreatic ductal adenocarcinoma. Abdom Radiol. 2020;45(11):3809–18.
26. Rong D, Mao Y, Hu W, Xu S, Wang J, He H, Li S, Zhang R. Intravoxel incoherent motion magnetic resonance imaging for differentiating metastatic and non-metastatic lymph nodes in pancreatic ductal adenocarcinoma. Eur Radiol. 2018;28(7):2781–9.
27. Harimoto N, Araki K, Hoshino K, Muranushi R, Hagiwara K, Ishii N, Tsukagoshi M, Igarashi T, Watanabe A, Kubo N, et al. Diffusion-Weighted MRI predicts lymph node metastasis and tumor aggressiveness in resectable pancreatic neuroendocrine tumors. World J Surg. 2020;44(12):4136–41.
28. Kurosawa J, Tawada K, Mikata R, Ishihara T, Tsuyuguchi T, Saito M, Shimofusa R, Yoshitomi H, Ohtsuka M, Miyazaki M, et al. Prognostic relevance of apparent diffusion coefficient obtained by diffusion-weighted MRI in pancreatic cancer. J Magn Reson Imaging. 2015;42(6):1532–7.
29. Shi Y, Liu B, Li X, Zhu H, Wei Y, Zhao B, Sun S, Sun Y, Hao C. Establishment of a multi-parameters MRI model for predicting small lymph nodes metastases (< 10 mm) in patients with resected pancreatic ductal adenocarcinoma. Abdom Radiol. 2022;47(9):3217–28.
30. Zhang D, Cui F, Zheng K, Li W, Liu Y, Wu C, Peng L, Yang Z, Chen Q, Xia C et al. Single-cell RNA sequencing reveals the process of CA19-9 production and dynamics of the immune microenvironment between CA19-9 (+) and CA19-9 (–) PDAC. *Chinese Med J-Peking* 2024.
31. Coppola A, La Vaccara V, Farolfi T, Asbun HJ, Boggi U, Conlon K, Edwin B, Ferrone C, Jonas E, Kokudo N, et al. Preoperative carbohydrate antigen 19.9 level predicts lymph node metastasis in resectable adenocarcinoma of the head of the pancreas: a further plea for biological resectability criteria. Int J Surg. 2024;110(10):6092–9.
32. Lundin J, Roberts PJ, Kuusela P, Haglund C. The prognostic value of preoperative serum levels of CA 19– 9 and CEA in patients with pancreatic cancer. Brit J Cancer. 1994;69(3):515–9.
33. Ge J, Li L, Ma Z, Jiang B, Yuan C, Wang H, Peng Y, Xiu D. A nomogram of preoperative predictors for occult metastasis in patients with PDAC during laparoscopic exploration. Gland Surg. 2021;10(1):279–89.

Publisher's note